Combination of Advanced Optical Modelling with Electrical Simulation for Performance Evaluation of Practical 4-terminal Perovskite/c-Si Tandem Modules

Zhang, Dong; Verhees, Wiljan; Dörenkämper, Maarten; Qiu, Weiming; Bakker, Klaas; Gutjahr, Astrid; Veenstra, Sjoerd; Gehlhaar, Robert; Paetzold, Ulrich W.; Soppe, Wim

DOI
10.1016/j.egypro.2016.07.039

Publication date
2016

Document Version
Final published version

Published in
Energy Procedia

Citation (APA)
Zhang, D., Verhees, W., Dörenkämper, M., Qiu, W., Bakker, K., Gutjahr, A., Veenstra, S., Gehlhaar, R., Paetzold, U. W., Soppe, W., Romijn, I., Geerligs, L. J., Aernouts, T., & Weeber, A. (2016). Combination of Advanced Optical Modelling with Electrical Simulation for Performance Evaluation of Practical 4-terminal Perovskite/c-Si Tandem Modules. *Energy Procedia*, *92*, 669-677. https://doi.org/10.1016/j.egypro.2016.07.039

Available online at www.sciencedirect.com

ScienceDirect

Energy Procedia 92 (2016) 669 – 677

Energy Procedia

6th International Conference on Silicon Photovoltaics, SiliconPV 2016

Combination of advanced optical modelling with electrical simulation for performance evaluation of practical 4-terminal perovskite/c-Si tandem modules

Dong Zhang[a,*], Wiljan Verhees[a], Maarten Dörenkämper[a], Weiming Qiu[b], Klaas Bakker[a], Astrid Gutjahr[a], Sjoerd Veenstra[a], Robert Gehlhaar[b], Ulrich W. Paetzold[b], Wim Soppe[a], Ingrid Romijn[a], L.J. Geerligs[a], Tom Aernouts[b] and Arthur Weeber[a,c]

[a]*ECN-Solliance, High Tech Campus 21, 5656 AE Eindhoven, the Netherlands*
[b]*IMEC-Solliance, Thin Film PV, Kapeldreef 75, B-3001 Leuven, Belgium*
[c]*TU Delft-Solliance, Photovoltaic Materials and Devices, Mekelweg 4, 2628 CD Delft, the Netherlands*

Abstract

The perovskite solar cell is considered a promising candidate as the top cell for high-efficiency tandem devices with crystalline silicon (c-Si) bottom cells, contributing to the cost reduction of photovoltaic energy. In this contribution, a simulation method, involving optical and electrical modelling, is established to calculate the performance of 4-terminal (4T) perovskite/c-Si tandem devices on a mini-module level. Optical and electrical characterization of perovskite and c-Si solar cells are carried out to verify the simulation parameters. With our method, the influence of transparent conductive oxide (TCO) layer thickness of perovskite top cells on the performance of tandem mini-modules is investigated in case of both tin-doped indium oxide (ITO) and hydrogen-doped indium oxide (IO:H). The investigation shows that optimization of TCO layer thickness and replacement of conventional ITO with highly transparent IO:H can lead to an absolute efficiency increase of about 1%. Finally, a practical assessment of the efficiency potential for the 4T perovskite/c-Si tandem mini-module is carried out, indicating that with a relatively simple 4T tandem module structure the efficiency of a single-junction c-Si mini-module (19.3%) can be improved by absolute 4.5%.

Peer review by the scientific conference committee of SiliconPV 2016 under responsibility of PSE AG.

Keywords: 4-termin**a**l; hybrid tandem; perovskite solar cell; simulation; transparent conductive oxide

* Corresponding author. Tel.: +31-88-515-4490; fax: +31 88-515-4480.
E-mail address: d.zhang@ecn.nl

Peer review by the scientific conference committee of SiliconPV 2016 under responsibility of PSE AG.
doi:10.1016/j.egypro.2016.07.039

1. Introduction

As nowadays the power conversion efficiency (*PCE*) of single-junction (SJ) crystalline silicon (c-Si) solar cells is approaching its practical limit of 26% [1], it is technically very challenging to realize any further improvement. This is implied by the fact that it took about 15 years to enhance the *PCE* of SJ c-Si cells from 25% [2] to 25.6% [3]. Application of the tandem device architecture, based on commercially successful c-Si solar cell technologies, may allow for an economically feasible route to further improve the performance of solar modules beyond the limits of SJ c-Si technology. Among the candidates for the wide-bandgap top cell of the tandem device, perovskite based solar cells are very promising [4] due to the advantages of high *PCE* [5], high absorption coefficients, a sharp absorption edge [6], a tunable bandgap [7, 8] and simple preparation process [9].

Theoretical calculations about the maximum attainable perovskite/c-Si tandem cell performance have been published by several authors [10, 11]. This contribution gives a practical evaluation of attainable 4-terminal (4T) pervoskite/c-Si module performances based on currently available commercial c-Si solar cells and small-scale perovskite solar cells processed in-house. The tandem module performance is calculated on mini-module level with verified optical and electrical simulations. With the simulation methods, the impact of TCO layer thickness of perovskite top cells on the module performance are investigated. The conventional tin doped indium oxide (ITO) is compared to the state-of-art hydrogen doped indium oxide (IO:H) as TCO of perovskite top cells, further exploring the possible *PCE* increase by optimizing the TCO. Finally the practically attainable *PCE* gain of the 4T perovskite/c-Si tandem mini-module compared to the SJ c-Si mini-modules is discussed.

2. Experiments

To verify the optical and electrical modelling, semi-transparent perovskite solar cells, c-Si cells and c-Si mini-modules are processed. Fabrication of semi-transparent perovskite solar cells start with ITO coated glass substrates which are ultrasonically cleaned for 10 minutes in detergent, deionized water and iso-propanol. The dense TiO_2 layer is made by spincoating a solution of 5 % titanium tetra-isopropoxide (TTIP) and 1% 1M HCl in iso-propanol. The obtained layers are annealed at 500 °C for 30 min. The perovskite precursor solution is made by mixing $Pb(CH_3CO_2)_2 \cdot 3H_2O$, $PbCl_2$ and methylammonium iodide (MAI) in dimethylformamide (DMF). The precursor solution is spincoated on top of the TiO_2 layer in a N_2 filled glovebox at 3000 rpm for 60 s. The perovskite layer is formed by annealing at 130 °C for 10 min [12]. On top of the perovskite layers a P3HT solution is spincoated (15 mg/ml in chlorobenzene doped with 5 µl 4-tert-butylpyridine (tBP) and 10 µl of a 170 mg/ml solution of lithium bistrifluoromethanesulfonamide (LiTFSi) in acetonitrile). To finish the devices a 160 nm thick ITO layer is deposited through a shadow mask by sputtering.

The metal-wrap-through (MWT) c-Si solar cells based on 6-inch n-type wafers are manufactured with mainstream industrial processes [13, 14] and then sliced by laser into 15.2 cm^2 squares for assembly of mini-modules. Laser processing is used to form via-holes by which the front side metal grid is wrapped through the wafer. The cell structure comprises a boron emitter, and a phosphorous Back Surface Field (BSF). Metallization is applied using screen-printing and is fired through the silicon nitride layers. Fig. 1(a) shows the picture of a c-Si mini-module with 4 MWT c-Si cells connected in series and this mini-module is designed to be the bottom sub-module of the tandem module. Fig.1(b) demonstrates the schematic layout of the designed 4T perovskite/c-Si tandem mini-module which is analyzed later with the simulation. This tandem module consists of a MWT c-Si bottom sub-module (Fig.1(a)) and interconnected perovskite top sub-module processed on the inner side of module glass. The Cu-coated backsheet is patterned for series connection of MWT cells and 4T wiring.

For characterization, the injection-level dependent *I-V* measurement for c-Si cells is done with the Neonsee solar simulator. The *I-V* characteristics of the perovskite cells is measured with a solar simulator built in-house inside the glovebox. External parameters of the semi-transparent perovskite cell and the SJ MWT c-Si mini-module processed in-house are listed in Table 1. The steady-state *PCE* of the cell is measured after it is kept at the maximum power point for 5 min. Regarding the reflectance and transmittance measurements, an Agilent Cary 5000 with integrating sphere is used. The external quantum efficiency (*EQE*) is measured with an Optosolar setup.

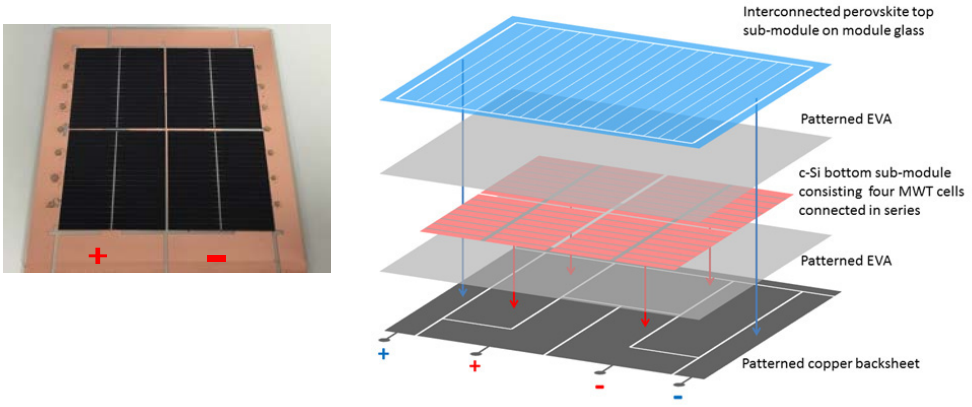

(a) (b)

Fig. 1. (a) Picture of the encapsulated MWT c-Si mini-module consisting of 4 MWT cells connected in series on Cu-coated backsheets and (b) the sketch of designed 4-terminal perovskite/c-Si tandem mini-module

Table 1. Performance of the semi-transparent perovskite cell and MWT c-Si minimodule measured at standard illumination conditions

Device	Aperture area (cm^2)	V_{oc} (V)	J_{sc} (mA/cm^2)	FF	*PCE*	Steady-state *PCE*
Semi-transparent perovskite cell	0.16	0.978	17.0	0.607	10.1% (backward scan)	8.8%
Encapsulated MWT c-Si mini-module with antireflective coating	64	2.61	9.77	0.756	19.3%	-

3. Method to analyze the performance of 4T perovskite/c-Si hybrid tandem mini-modules

3.1. Optical simulation for calculating the short-circuit current density

The method to analyse the performance of 4T hybrid tandem mini-modules is mainly based on advanced optical simulation combined with solving diode equations. Optical simulation is carried out with the GenPro4 program [4, 15, 16] developed at Delft University of Technology, aiming to calculate the short-circuit current density (J_{sc}) of solar cells. With the optical simulation, the reflectance (R), transmittance (T) and absorbance of each layer (A) of solar cells can be calculated. It is assumed that the active-area short-circuit current density (J_{sc}) approximates the current density (J) calculated from the absorbance of active layers ($CH_3NH_3PbI_3$ (MAPI) layer for perovskite cells (J_{MAPI}) and the c-Si "layer" for c-Si cells (J_{cSi})), which is expressed by the following equations:

$$J_{sc1} \approx J_{MAPI} = q\int_{300}^{1200} A_{MAPI}(\lambda)\phi(\lambda)d\lambda \text{ and } J_{sc2} \approx J_{cSi} = q\int_{300}^{1200} A_{cSi}(\lambda)\phi(\lambda)d\lambda\,, \quad (1)$$

where J_{sc1} and J_{sc2} are the active-area J_{sc}'s of perovskite top and c-Si bottom cells, λ is the wavelength, q is the elementary charge and $\phi(\lambda)$ is the photon flux of the AM1.5 solar spectrum. Since reflection and parasitic absorption losses of solar cells are taken into account, this assumption is acceptable for estimating J_{sc} if the thickness of the active layer is smaller than the collection length of minority carriers. To validate the optical simulation and the assumption of J_{sc} calculation, optical and electrical measurements are carried out for both perovskite and c-Si solar cells and compared with the simulation results. Fig. 2(a) shows that the simulated R and T of semi-transparent perovskite cells have a good agreement with the measurements. The *I-V* characterization of perovskite cells

processed in this study shows that calculated J_{MAPI} (17.7 mA/cm^2) approximates the measured J_{sc1} (17 mA/cm^2). With respect to c-Si cells demonstrated in Fig. 2(b), all the light absorption in the c-Si wafer is able to contribute to the current except the free carrier absorption (FCA) in highly doped emitter and back surface field (BSF). Therefore, the FCA in the emitter and BSF, which causes parasitic absorption losses, is differentiated from the rest of light absorption in the c-Si wafer. Based on the measured doping concentration and sheet resistance, two FCA layers corresponding to the emitter and BSF are defined in the optical structure to indicate FCA losses at wavelengths over 1 μm [17]. The FCA is determined by the absorption coefficients calculated by the following equations [18]:

$$\alpha_{FCA,B} = 1.8e-9 \cdot N \cdot \lambda^{2.18} \text{ and } \alpha_{FCA,P} = 1.68e-6 \cdot N \cdot \lambda^{2.88}, \quad (2)$$

where $\alpha_{FCA,B}$ and $\alpha_{FCA,P}$ correspond to the absorption coefficient of the boron-doped emitter region and phosphor-doped BSF region, N is the free carrier concentration. As demonstrated in Fig. 2(b), the simulated reflectance fits well with the measurements. Furthermore, Fig. 3 shows the simulated absorbance spectrum is in good agreement with the *EQE* measured at the active area of the MWT cell, suggesting that J_{sc2} approximates J_{cSi} and further validating the accuracy of the assumption in Eq. 1.

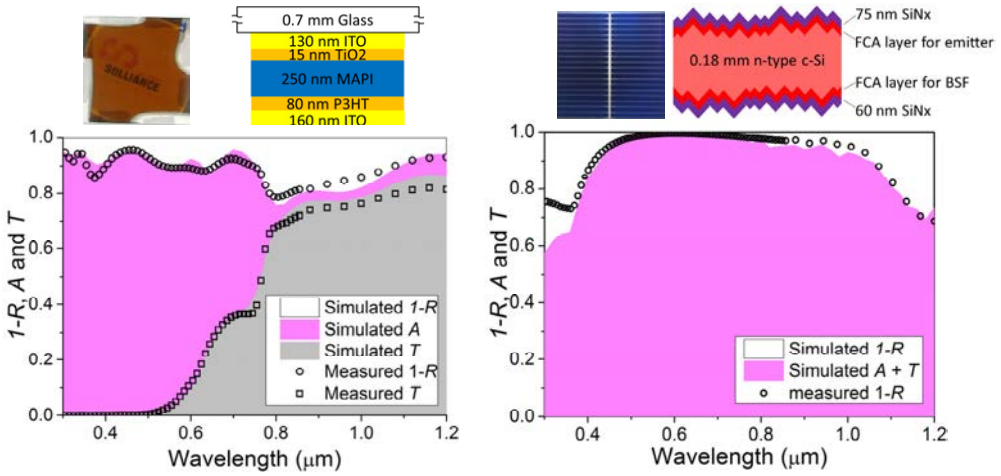

(a) (b)

Fig. 2. Device picture, the optical structure and comparison between the simulated and measured reflectance, absorbance and transmittance spectra for (a) semi-transparent perovskite cells and (b) MWT c-Si cells

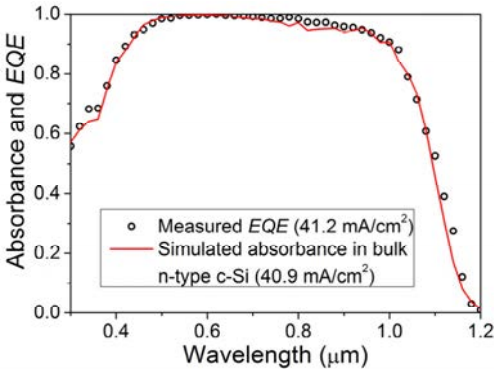

Fig. 3. Comparison between the simulated absorbance spectrum of c-Si "layer"and measured *EQE* spectrum of MWT c-Si cells.

3.2. Modified one-diode equation for calculating open-circuit voltage and fill factor of c-Si mini-modules

In tandem devices, c-Si bottom cells operate at lower injection levels than the standard irradiance condition. Depending on the optical structure of tandem devices and the materials used in the top cells, the injection level for the c-Si bottom cell varies. The injection-level change for a c-Si bottom cell has direct impact on its short-circuit current (I_{sc2}). The I_{sc2} is related to J_{sc2} by the equation:

$$I_{sc2} = J_{sc2} \cdot a_{Si} \cdot (1-c)\,, \tag{3}$$

where a_{Si} is the area of c-Si cells, c is the area fraction of the metal grid and J_{sc2} can be calculated from Eq. 1. The variation of I_{sc2} leads to the change of open-circuit voltage (V_{oc2}) and fill factor (FF_2) of c-Si cells, which can be basically calculated with the one-diode equation. However, with the diode parameters all kept constant, the injection-level dependence of c-Si cells cannot be accurately calculated. Chegaar et al. has reported the injection-level dependence of the diode parameters [19] for multicrystalline Si cells. Compared to what Chegaar et al. reported, Fig. 4 shows that the injection-level dependence of three diode parameters for the MWT c-Si mini-module (picture of Fig. 1(a)) follow the same trend, that is, the saturation current (I_0) increases exponentially with I_{sc2}, the ideality factor (n) increases linearly with I_{sc2}, the series resistance (R_s) remains constant. However, a slight difference is that instead of following one linear equation, the shunt resistance (R_{sh}) remains constant at the I_{sc2} of over 0.35 A. With the introduction of the injection-level-dependent diode parameters, the one-diode equation is modified as follows :

$$I = I_{sc2} - I_0(I_{sc2}) \cdot (\exp(\frac{V + I \cdot R_s}{n(I_{sc2}) \cdot k \cdot T}) - 1) - \frac{V + I \cdot R_s}{R_{sh}(I_{sc2})}\,, \tag{4}$$

where k is the Boltzmann constant and T is the absolute temperature. Fig. 5 shows that with Eq. 4, V_{oc2} and FF_2 of the MWT c-Si mini-module at different injection levels can be accurately calculated.

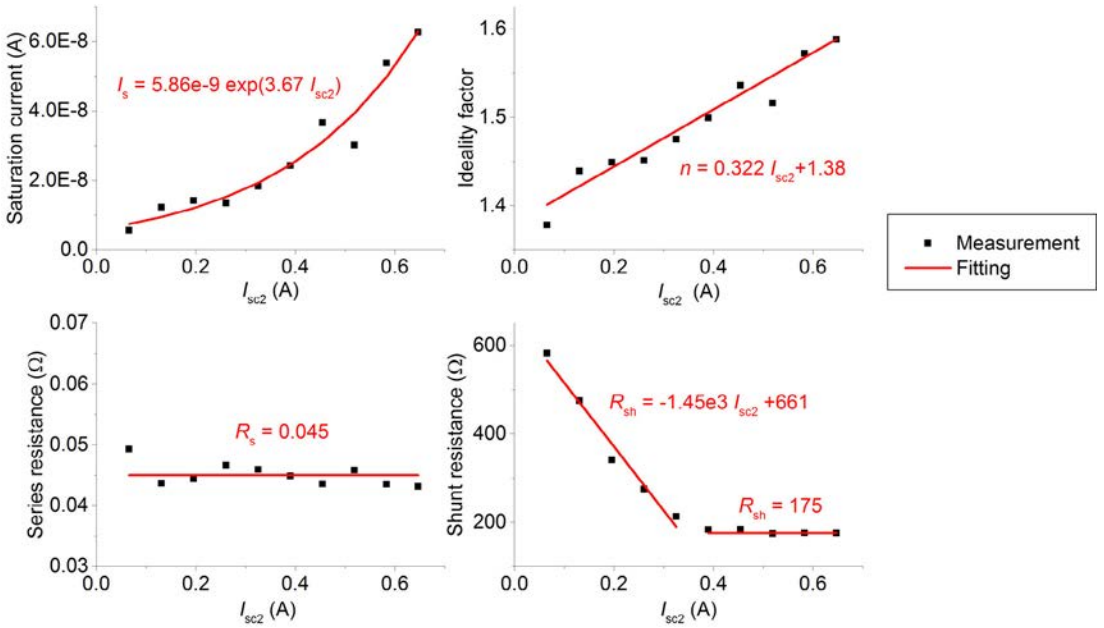

Fig. 4. Injection dependence of diode parameters for the MWT c-Si mini-module.

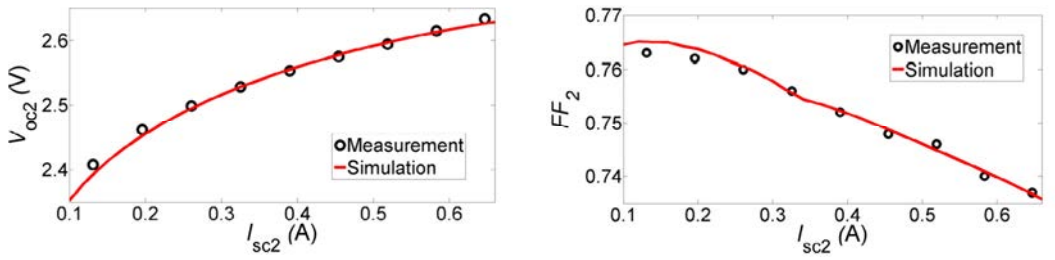

(a) (b)

Fig. 5. Comparison of (a) V_{oc2} and (b) FF_2 calculated with modified one-diode equations for the MWT c-Si mini-module to the results measured at different injection levels.

3.3. Calculation of 4-terminal tandem mini-module PCE

In the 4T tandem modules, the perovskite top cells are interconnected and fully rely on the TCO for current transport. In addition to the parasitic absorption losses that have been considered in the optical simulation, the resistance loss resulting from front and rear TCO electrodes cannot be neglected [20, 21]. This resistance loss (r) is calculated by the equation:

$$r = \frac{\int_0^w (J_{m1} \cdot x \cdot L)^2 \cdot \frac{\rho}{d_1 \cdot L} dx}{V_{m1} \cdot J_{m1} \cdot w \cdot L} + \frac{\int_0^w (J_{m1} \cdot x \cdot L)^2 \cdot \frac{\rho}{d_2 \cdot L} dx}{V_{m1} \cdot J_{m1} \cdot w \cdot L} \approx \frac{J_{sc1} \cdot \rho \cdot w^2}{3 \cdot V_{oc1}} \left(\frac{1}{d_1} + \frac{1}{d_2}\right), \quad (5)$$

where J_{m1} and V_{m1} are the current density and voltage at the maximum power point, ρ is the resistivity of TCO, w is the cell width (5 mm), d_1 *and* d_2 are the front and rear TCO layer thickness respectively and L is the length of the cell (8 cm). The *PCE* of 4T tandem modules (η_{4T}) is expressed by the equation:

$$\eta_{4T} = \frac{(1-f) \cdot (1-r) \cdot V_{oc1} \cdot J_{sc1} \cdot FF_1}{100} \cdot 100\% + \frac{V_{oc2} \cdot I_{sc2} \cdot FF_2}{100 \cdot a_A} \cdot 100\%, \quad (6)$$

where f is the fraction of the dead area (2%) in perovskite top sub-modules and a_A is the aperture area of the tandem mini-modules (64 cm^2) and V_{oc1} and FF_1 are the open-circuit voltage and fill factor of the perovskite top cell for which the measured values or the literature values are used in the analysis.

4. Results and discussion

4.1. Impacts of TCO on the performance of tandem mini-modules

Based on the 4-terminal tandem module architecture , the layer stack for optical simulation is defined as shown in Fig. 6(a). Two optimizations are implemented into the studied module structure. One is the application of the antireflective texture developed in-house with imprint lithography. The imprinted texture is a replica of random pyramids on textured c-Si wafer, reducing the reflection losses and scattering the light to enhance the light absorption of solar cells. The other optimization is that the MAPI layer thickness is increased up to 330 nm as suggested by Liu et al. [22] to increase the photocurrent of the perovskite top cell without degradation of V_{oc} and *FF*. With the methodology introduced in section 3, the impact of TCO layer thickness on tandem module performance is investigated. In addition, in-house ITO is compared to published state-of-art IO:H [23] as TCO in perovskite top cells to further explore the *PCE* potential of the tandem module. Fig. 6(b) demonstrates the optical constants of ITO and IO:H, indicating that IO:H has lower absorption in ultraviolet (UV) and near infrared (NIR) than ITO at the

same layer thickness. Although IO:H has lower free carrier density, implied by the low NIR absorption, IO:H has no larger resistivity than ITO due to its higher mobility. Fig. 7(a) shows the *PCE* of the tandem modules as a function of front and rear ITO layer thickness. The optimum front ITO layer thickness is about 120 nm. However, for the rear ITO, the layer thickness can be over 250 nm. The difference in desired front and rear ITO layer thickness originates from their different optical characteristics of the adjacent layers. Since the light is incident from the front ITO, its parasitic absorption is more relevant for a larger part of the solar spectrum compared to the rear ITO. As the front ITO layer thickness rises, the resistance loss decreases while the parasitic absorption loss increases. At the front ITO layer thickness of below 120 nm, the decrease of the resistance loss overruns the increase of the parasitic absorption loss as the front ITO layer thickness rises, leading to the *PCE* improvement. At above 120 nm, the increase of the parasitic absorption loss dominates and hence the overall *PCE* of the tandem module decreases as the front ITO layer thickness rises. For the rear ITO layer, its related resistance loss dominates and hence the much thicker layer is preferred. Similar to ITO, the module *PCE* increases with the rear IO:H layer thickness as shown in Fig. 7(b). However, with respect to the front IO:H, the increase of the parasitic absorption loss cannot overrun the decrease of the resistance loss as the layer thickness rises. This is mainly due to the very low parasitic absorption of IO:H. With respect to the *PCE* of tandem modules, variation of the front and rear TCO layer thickness between 100 nm and 300 nm can lead to an absolute *PCE* difference of 0.5%. Replacement of ITO with IO:H results in an additional *PCE* gain of absolute 0.5%.

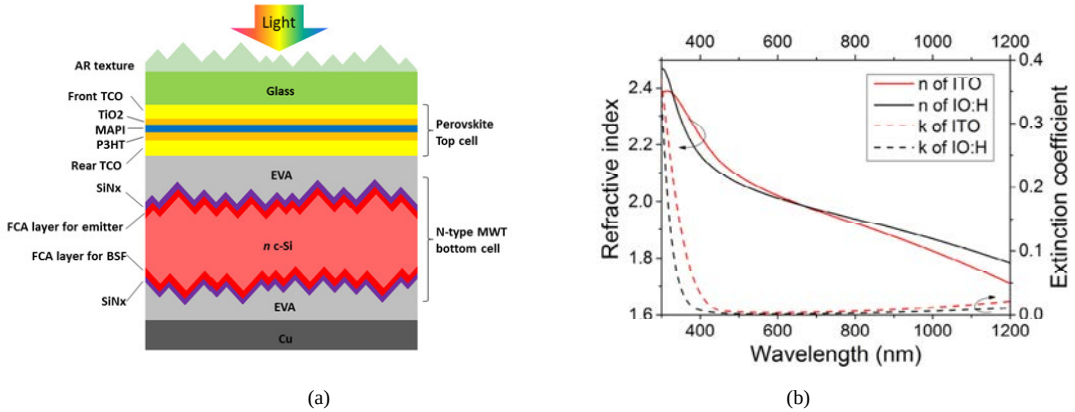

Fig. 6. (a) Schematic layer stack of the 4T perovskite/c-Si tandem mini-module for optical simulation and (b) optical constants of the ITO and IO:H (the resistivity of ITO and IO:H is 4.3e-4 Ω·cm and 2.7e-4 Ω·cm respectively)

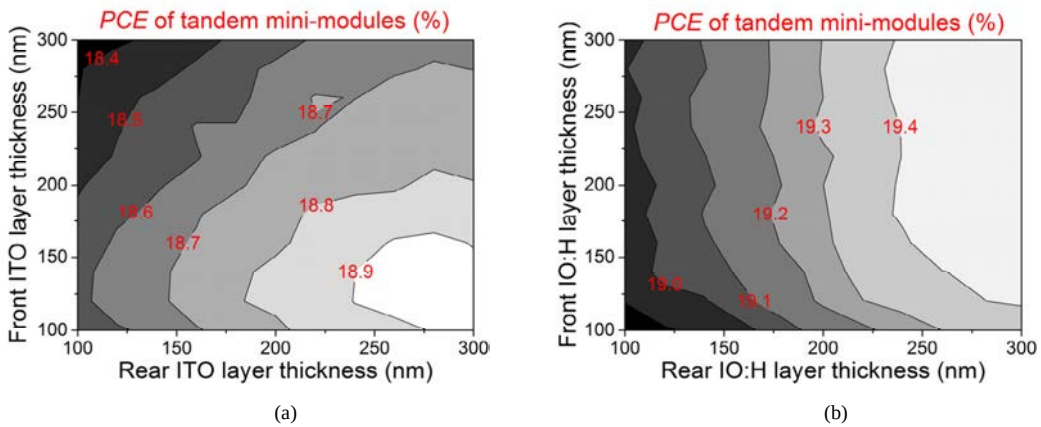

Fig. 7. *PCE* of the 4T tandem mini-module as a function of front and rear TCO layer thickness in case of (a) ITO and (b) IO:H. The V_{oc} and *FF* of perovskite cells are 0.978 V and 60.7% from Table 1.

4.2. Assessment of possible PCE gain for 4T perovskite/c-Si tandem mini-modules

Based on investigation of TCO presented in section 4.1, front and rear IO:H layer thicknesses of 180 nm and 240 nm respectively are used in the structure of Fig. 6(a) for the calculation of tandem module *PCE* to investigate the possible *PCE* gain. The reason for choosing those layer thickness is that further increase of the layer thickness cannot leads to a noticeable *PCE* enhancement. Compared to the SJ MWT c-Si mini-module with a *PCE* of 19.3% (Table 1), the absolute *PCE* gain is plotted as a function of V_{oc} and *FF* of the perovskite top cell . As shown in Fig. 8, the V_{oc} and *FF* of perovskite cells achieved in-house at the current stage (yellow circle) can lead to about 0.5% *PCE* gain. With the highest V_{oc} and *FF* that is published in the literature for the semi-transparent perovskite cells (yellow square) [9], an absolute *PCE* gain as high as 4.5% is attainable.

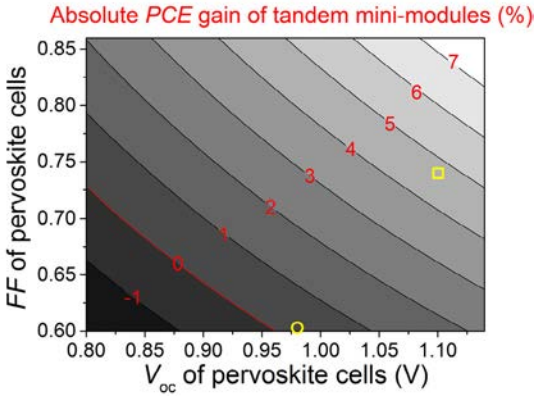

Fig. 8. *PCE* of the designed tandem mini-module as a function of V_{oc} and *FF* of the perovskite top cell in case of IO:H used as TCO. The red line indicates the required V_{oc} and *FF* of perovskite cells to break even. The yellow circle indicates the V_{oc} and *FF* achieved in-house (0.978 V and 60.7%) and the yellow square corresponds to the V_{oc} and *FF* of semi-transparent perovskite cells reported in the literature (1.104 V and 73.6%).

5. Conclusion

In this contribution, a simulation method to calculate the performance of 4T perovskite/c-Si tandem modules is introduced and can be used for optimization of tandem module structures. To validate this simulation method, optical modelling of both perovskite and c-Si cells is experimentally verified. To accurately calculate the performance of MWT c-Si cells at different injection levels, the one-diode equation is modified by introducing injection-level dependent diode parameters. With the proposed simulation method, the impacts of TCO on the performance of tandem modules are investigated. Variation of front and rear TCO layer thicknesses changes the parasitic absorption and resistance losses of tandem modules, leading to an absolute *PCE* difference of 0.5%. The state-of-art IO:H can result in an absolute *PCE* increase of 0.5% compared to in-house ITO. At last, compared to the *PCE* of 19.3% for encapsulated SJ MWT c-Si mini-modules, the simulation in this study shows the semi-transparent perovskite cells processed in-house can lead to an absolute *PCE* gain of 0.5% with the tandem module structure. Furthermore, with highest reported V_{oc} and *FF* achieved in semi-transparent perovskite cells, an absolute *PCE* gain of 4.5% should be feasible.

Acknowledgements

This work is funded by TKI Hi Eff and TO2 Solliance projects. Authors would like to thank Rudi Santbergen at TU Delft and Yu Wu, Agnes Mewe, John van Roosmalen and Gianluca Coletti at ECN for their helpful discussion.

References

[1] Swanson RM. Approaching the 29% limit efficiency of silicon solar cells. in Proceedings of 31st IEEE Photovoltaic Specialists Conference 2005. 889–894.

[2] Zhao J, Wang A, Green MA. 24.5% efficiency silicon PERT cells on MCZ substrates and 24.7% efficiency PERL cells on FZ substrates. Prog Photovoltaics Res Appl 1999; 7:471-474.

[3] Masuko K, Shigematsu M, Hashiguchi T, Fujishima D, Kai M, Yoshimura N, Yamaguchi T, Ichihashi Y, Mishima T, Matsubara N, Yamanishi T, Takahama T, Taguchi M, Maruyama E, Okamoto S, Achievement of more than 25%; conversion efficiency with crystalline silicon heterojunction solar cell. IEEE J Photovoltaics 2014; 4:1433-1435.

[4] Zhang D, Soppe W, Schropp RE. Design of 4-terminal solar modules combining thin-film wide-bandgap top cells and c-Si bottom cells. Energy Procedia 2015; 77: 500-507.

[5] Green MA, Emery K, Hishikawa Y, Warta W, Dunlop ED, Solar cell efficiency tables (version 45), Prog Photovoltaics Res Appl 2015; 23:1-9.

[6] De Wolf S, Holovsky J, Moon SJ, Löper P, Niesen B, Ledinsky M, Haug FJ, Yum JH, Ballif C. Organometallic halide perovskites: Sharp optical absorption edge and its relation to photovoltaic performance. J Phys Chem Lett. 2014; 5:1035-1039.

[7] Eperon GE, Stranks SD, Menelaou C, Johnston MB, Herz LM, Snaith HJ. Formamidinium lead trihalide: a broadly tunable perovskite for efficient planar heterojunction solar cells. Energy Environ Sci 2014; 7:982-988.

[8] McMeekin DP, Sadoughi G, Rehman W, Eperon GE, Saliba M, Hörantner MT, Haghighirad A, Sakai N, Korte L, Rech B, Johnston MB, Herz LM, Snaith HJ. A mixed-cation lead mixed-halide perovskite absorber for tandem solar cells. Science 2016; 351:151-155.

[9] Fu F, Feurer T, Jager T, Avancini E, Bissig B, Yoon S, Buecheler S, Tiwari AN. Low-temperature-processed efficient semi-transparent planar perovskite solar cells for bifacial and tandem applications. Nat Commun 2015; 6:1.

[10] White T, Lal N, Catchpole K. Tandem solar cells based on high-efficiency c-Si bottom cells: Top cell requirements for >30% efficiency. IEEE J Photovoltaics 2014; 4:208-214.

[11] Löper P, Niesen B, Moon SJ, Martin de Nicolas S, Holovsky J, Remes Z, Ledinsky M, Haug FJ, Yum JH, De Wolf S, Ballif C. Organic inorganic halide perovskites: Perspectives for silicon-based tandem solar cells. IEEE J Photovoltaics 2014; 4:1545–1551.

[12] Qiu W, Merckx T, Jaysankar M, Masse de la Huerta C, Rakocevic L, Zhang W, Paetzold UW, Gehlhaar R, Froyen L, Poortmans J, Cheyns D, Snaith HJ, Heremans P. Pinhole-free perovskite films for efficient solar modules. Energy Environ Sci 2016; 9:484-489.

[13] Guillevin N, Heurtault B, Geerligs L, Weeber A. Development towards 20% efficient Si MWT solar cells for low-cost industrial production. Energy Procedia 2011; 8:9-16.

[14] Guillevin N, Gutjahr A, Geerligs L, Anker J, Bennett EBI, Koppes M, Kossen E, Okel L, Slooff L, Broek K, Späth M, Tool C, Aken BV, Romijn I, Wang J, Wang Z, Zhai J, Wan Z, Tian S, Hu Z, Li G, Yu B, Xiong J. High efficiency n-type metal-wrap-through cells and modules using industrial processes. in Proceedings of the 29th European Photovoltaic Solar Energy Conference, 2014.

[15] Zhang D, Digdaya I, Santbergen R, van Swaaij RACMM, Bronsveld P, Zeman M, van Roosmalen J, Weeber A. Design and fabrication of a SiOx/ITO double-layer anti-reflective coating for heterojunction silicon solar cells. Sol Energy Mater Sol Cells 2013; 117:132-138.

[16] Zhang D, Deligiannis D, Papakonstantinou G, van Swaaij RACMM, Zeman M. Optical enhancement of silicon heterojunction solar cells with hydrogenated amorphous silicon carbide emitter. IEEE J Photovoltaics 2014; 4:1326-1330.

[17] Santbergen R, van Zolingen R. The absorption factor of crystalline silicon PV cells: A numerical and experimental study. Sol Energy Mater Sol Cells 2008; 92:432-444.

[18] Baker-Finch SC, McIntosh KR, Yan D, Fong KC, Kho TC. Near-infrared free carrier absorption in heavily doped silicon. J. Appl. Phys. 2014; 116:063106.

[19] Chegaar M, Hamzaoui A, Namoda A, Petit P, Aillerie M, Herguth A. Effect of illumination intensity on solar cells parameters. Energy Procedia 2013; 36:722-729.

[20] Koishiyev GT, Sites JR. Impact of sheet resistance on 2-d modeling of thin-film solar cells. Sol Energy Mater Sol Cells 2009; 93:350-354.

[21] Löper P, Moon SJ, Martin de Nicolas S, Niesen B, Ledinsky M, Nicolay S, Bailat J, Yum JH, De Wolf S, Ballif C. Organic-inorganic halide perovskite/crystalline silicon four-terminal tandem solar cells. Phys Chem Chem Phys 2015; 17:1619-1629.

[22] Liu D, Gangishetty MK, Kelly TL. Effect of CH3NH3PbI3 thickness on device efficiency in planar heterojunction perovskite solar cells. J Mater Chem A 2014; 2:19873-19881.

[23] Macco B, Wu Y, Vanhemel D, Kessels WMM. High mobility In2O3:H transparent conductive oxides prepared by atomic layer deposition and solid phase crystallization. Phys Status Solidi RRL 2014; 8:987-990.